Supplementary Information

Buckling-induced F-actin fragmentation modulates contraction of active cytoskeletal networks

Jing Li¶, Thomas Biel¶, Pranith Lomada¶, Qilin Yu, Taeyoon Kim*

Weldon School of Biomedical Engineering, Purdue University
206 S. Martin Jischke Drive, West Lafayette, IN 47907, USA

"¶" indicates equal contribution

"*" indicates a corresponding author

Brownian dynamics via the Langevin equation

In the model, F-actins are comprised of serially-connected cylindrical segments with barbed and pointed ends. ACPs consist of a pair of cylindrical segments. Each motor is modeled after myosin thick filaments; a motor has a backbone structure with 8 arms, and each of the arms represents 8 myosin heads. Displacements of the segments are governed by the Langevin equation with inertia neglected:

$$\mathbf{F}_i - \zeta_i \frac{\mathrm{d}\mathbf{r}_i}{\mathrm{d}t} + \mathbf{F}_i^{\mathrm{T}} = 0 \tag{1}$$

where $\mathbf{r}_i$ is a position vector of the ith element, ζ_i is a drag coefficient, t is time, $\mathbf{F}_i$ is a deterministic force, and $\mathbf{F}_i^{\mathrm{T}}$ is a stochastic force satisfying the fluctuation-dissipation theorem [1]:

$$\left\langle \mathbf{F}_i^{\mathrm{T}}(t)\mathbf{F}_j^{\mathrm{T}}(t) \right\rangle = \frac{2k_{\mathrm{B}}T\zeta_i\delta_{ij}}{\Delta t}\boldsymbol{\delta} \tag{2}$$

where δ_{ij} is the Kronecker delta, $\boldsymbol{\delta}$ is a second-order tensor, and $\Delta t = 1.5\times10^{-5}$ s is a time step. Drag coefficients are calculated using an approximated form for a cylindrical object [2]:

$$\zeta_i = 3\pi\mu r_{\mathrm{c},i}\frac{3 + 2r_{0,i} / r_{\mathrm{c},i}}{5} \tag{3}$$

where μ is the viscosity of medium, and $r_{0,i}$ and $r_{\mathrm{c},i}$ are length and diameter of a segment, respectively. Positions of all the cylindrical segments are updated using Euler integration scheme:

$$\mathbf{r}_i(t+\Delta t) = \mathbf{r}_i(t) + \frac{\mathrm{d}\mathbf{r}_i}{\mathrm{d}t}\Delta t = \mathbf{r}_i(t) + \frac{1}{\zeta_i}\left(\mathbf{F}_i + \mathbf{F}_i^{\mathrm{T}}\right)\Delta t \tag{4}$$

Note that we employed a 10-fold higher value for μ than that used in our previous study where influences of F-actin severing on rheological behaviors of cross-linked actin networks were investigated.[3] Since simulations of aggregating networks in this study tend to significantly slow down later times, an increase in Δt is necessary for exploring wide parametric spaces, which can be achieved by the increase in μ in an over-damped system. It was verified that network contraction in four representative cases among data shown in Fig. 3 is similar between the cases with $\mu = 8.6\times10^{-1}$ [kg/m·s] and those with $\mu = 8.6\times10^{-2}$ [kg/m·s] (Fig. S7).

Deterministic forces

Deterministic forces include extensional forces maintaining equilibrium lengths, bending forces maintaining equilibrium angles, and repulsive forces accounting for volume-exclusion effects between actin segments. The extensional and bending forces originate from harmonic potentials:

$$U_{\mathrm{s}} = \frac{1}{2}\kappa_{\mathrm{s}}(r - r_0)^2 \tag{5}$$

$$U_{\mathrm{b}} = \frac{1}{2}\kappa_{\mathrm{b}}\left(\theta - \theta_0\right)^2 \tag{6}$$

where κ_{s} and κ_{b} are extensional and bending stiffnesses, r and r_0 is instantaneous and equilibrium lengths of cylindrical segments, and θ and θ_0 are instantaneous and equilibrium angles formed by adjacent segments. An equilibrium length of actin segments ($r_{0,\mathrm{A}}$ = 140 nm) and an equilibrium angle formed by two adjacent actin segments ($\theta_{0,\mathrm{A}}$ = 0 rad) are regulated by extensional ($\kappa_{\mathrm{s,A}}$) and bending stiffnesses of actins ($\kappa_{\mathrm{b,A}}$), respectively. The reference value of $\kappa_{\mathrm{b,A}}$ corresponds to the persistence length of 9 μm.[4] An equilibrium length of ACP arms ($r_{0,\mathrm{ACP}}$ = 23.5 nm) and an equilibrium angle formed by two arms of each ACP ($\theta_{0,\mathrm{ACP}}$ = 0 rad) are maintained by extensional ($\kappa_{\mathrm{s,ACP}}$) and bending stiffnesses of ACPs ($\kappa_{\mathrm{b,ACP}}$), respectively. An equilibrium length of motor backbone segments ($r_{\mathrm{s,M1}}$= 42 nm) and an equilibrium angle formed by adjacent backbone segments ($\theta_{0,\mathrm{M}}$ = 0 rad) are maintained by extensional ($\kappa_{\mathrm{s,M1}}$) and bending stiffnesses ($\kappa_{\mathrm{b,M}}$), respectively. The value of $\kappa_{\mathrm{s,M1}}$ is equal to that of $\kappa_{\mathrm{s,A}}$, whereas the value of $\kappa_{\mathrm{b,M}}$ is larger than that of $\kappa_{\mathrm{b,A}}$. Extension of each motor arm is regulated by the two-spring model with stiffnesses of transverse ($\kappa_{\mathrm{s,M2}}$) and longitudinal springs ($\kappa_{\mathrm{s,M3}}$). The transverse spring maintains an equilibrium distance ($r_{0,\mathrm{M2}}$ = 13.5 nm) between an endpoint of a motor backbone and actin segment where the arm of the motor binds, whereas the longitudinal spring helps maintaining a right angle between the motor arm and the actin segment ($r_{0,\mathrm{M3}}$ = 0 nm). Forces exerted on actin segments by bound ACPs and motors are distributed onto the barbed and pointed ends of the actin segments as described in our previous work. A repulsive force is represented by a harmonic potential[5]:

$$U_{\mathrm{r}} = \begin{cases} \frac{1}{2}\kappa_{\mathrm{r}}\left(r_{12} - r_{\mathrm{c,A}}\right)^2 & \text{if} \quad r_{12} < r_{\mathrm{c,A}} \\ 0 & \text{if} \quad r_{12} \geq r_{\mathrm{c,A}} \end{cases} \tag{7}$$

where κ_{r} is strength of repulsive force, and r_{12} is the minimum distance between two actin segments.

Dynamics of ACPs

ACPs bind to binding sites located every 7 nm on actin segments with no preference of contact angle. ACPs also unbind from F-actin in a force-dependent manner following Bell's equation[6]:

$$k_{\mathrm{u,ACP}} = \begin{cases} k_{\mathrm{u,ACP}}^{0} \exp\left(\dfrac{\lambda_{\mathrm{u,ACP}}\left|\vec{F}_{\mathrm{s,ACP}}\right|}{k_{\mathrm{B}}T}\right) & \text{if } r \geq r_{0,\mathrm{ACP}} \\ k_{\mathrm{u,ACP}}^{0} & \text{if } r < r_{0,\mathrm{ACP}} \end{cases} \tag{8}$$

where $k^0_{\mathrm{u,ACP}}$ is the zero-force unbinding rate, $\lambda_{\mathrm{u,ACP}}$ represents a sensitivity to applied force, and $k_\mathrm{B}T$ is thermal energy. The references values of $k^0_{\mathrm{u,ACP}}$ (= 0.115 s^{-1}) and $\lambda_{\mathrm{u,ACP}}$ (= 1.04×10^{-10} m) correspond to filamin A.[7]

Although we assumed the slip-bond nature of ACPs in this study, we also tested influences of force sensitivity of ACP unbinding on network contraction. We measured network contraction in four representative cases among data shown in Fig. 3 with catch-bond ACPs ($\lambda_{\mathrm{u,ACP}}$ = -0.115 s^{-1}) or with ideal-bond ACPs ($\lambda_{\mathrm{u,ACP}}$ = 0) (Fig. S8). We observed that with a reference value of bending stiffness ($\kappa_{\mathrm{b,A}}$), the extent of network contraction varies only slightly due to a change in the force sensitivity. By contrast, with large $\kappa_{\mathrm{b,A}}$, contraction is significantly greater in networks with catch-bond ACPs or ideal-bond ACPs. If $\kappa_{\mathrm{b,A}}$ is large, a network resists contraction stronger, resulting in a larger amount of forces on each ACP. If ACPs behave as a slip-bond, this large force accelerates unbinding events of ACPs, so network connectivity is impaired, leading to smaller network contraction. By contrast, if ACPs do not behave as a slip-bond, network connectivity is maintained, leading to large network contraction.

Dynamics of motors

Motor arms bind to binding sites on actin segments at a rate of $40N_\mathrm{h}$ s^{-1}, where N_h = 8 is the number of myosin heads represented by each arm. Walking ($k_{\mathrm{w,M}}$) and unbinding rates ($k_{\mathrm{u,M}}$) of the motor arms are regulated by the parallel cluster model to mimic the mechanochemical cycle of non-muscle myosin II.[8,9] Details of implementation and benchmarking of the parallel cluster model in our models are extensively described in our previous study.[10] Note that $k_{\mathrm{w,M}}$ and $k_{\mathrm{u,M}}$ are lower with higher applied load since motors exhibit a catch-bond behavior. Unloaded walking velocity and stall force of motors are set to ~140 nm/s and ~5.7 pN, respectively.

To check generality of results in this study, we tested effects of $k_{\mathrm{w,M}}$ on network contraction in four representative cases among data shown in Fig. 3 by varying it from 70 nm/s to 350 nm/s. It was observed that the extent of network contraction is almost independent of $k_{\mathrm{w,M}}$ (Fig. S9), whereas average contraction rate is proportional to $k_{\mathrm{w,M}}$, which is consistent with an experiment.[11]

Determination of parameters for the F-actin severing model

In our previous study[3], we determined the values of zero-angle severing rate constant ($k^0_{\mathrm{s,A}}$) and sensitivity to bending angles ($\lambda_{\mathrm{s,A}}$) in Eq. 1 by comparing with an in vitro experiment. In the experiment, they measured distribution of angles where thermally fluctuating F-actin was spontaneously severed. We ran a simulation with thermally fluctuating F-actins and found the values of $k_{\mathrm{s,A}}^{0}$ and $\lambda_{\mathrm{s,A}}$ resulting in similar distribution of severing angles. In the simulation, we observed severing angles only up to 68° since frequency of very large bending angles was very small partially due to the discretization of F-actin into cylindrical segments. However, large bending angles above 68° can easily occur if F-actin experiences buckling events in response to external mechanical stimuli or as a result of motor activity. Considering that the local accumulation of stress is known to be a molecular origin of the filament severing, an exponential increase in the severing rate due to an increase in a bending angle seems valid for bending angles above 68°. Note that Eq. 1 allows F-actin without any bending to be severed. However, a severing rate for 0° is negligibly small, so it is not likely that F-actin is severed without bending during simulations or within physiologically relevant time scales.

Table S1. List of parameters employed in the model.

Symbol	Definition	Value
$r_{0,\mathrm{A}}$	Length of an actin segment	1.4×10^{-7} [m]
$r_{\mathrm{c,A}}$	Diameter of an actin segment	7.0×10^{-9} [m] [12]
$\theta_{0,\mathrm{A}}$	Bending angle formed by adjacent actin segments	0 [rad]
$\kappa_{\mathrm{s,A}}$	Extensional stiffness of F-actin	1.69×10^{-2} [N/m]
$\kappa_{\mathrm{b,A}}$	Bending stiffness of F-actin	2.64×10^{-19} [N·m] [4]
$r_{0,\mathrm{ACP}}$	Length of an ACP arm	2.35×10^{-8} [m] [13]
$r_{\mathrm{c,ACP}}$	Diameter of an ACP arm	1.0×10^{-8} [m]
$\theta_{0,\mathrm{ACP}}$	Bending angle formed by two ACP arms	0 [rad]
$\kappa_{\mathrm{s,ACP}}$	Extensional stiffness of ACP	2.0×10^{-3} [N/m]
$\kappa_{\mathrm{b,ACP}}$	Bending stiffness of ACP	0 [N·m]
$r_{0,\mathrm{M1}}$	Length of motor backbone segment	4.2×10^{-8} [m]
$\theta_{0,\mathrm{M}}$	Bending angle formed by adjacent segments constituting motor backbone	0 [rad]
$\kappa_{\mathrm{s,M1}}$	Extensional stiffness of motor backbone	1.69×10^{-2} [N/m]
$\kappa_{\mathrm{b,M}}$	Bending stiffness of motor backbone	5.07×10^{-18} [N·m]
$r_{0,\mathrm{M2}}$	Length of a motor arm	1.35×10^{-8} [m]
$r_{\mathrm{c,M}}$	Diameter of a motor arm	1.0×10^{-8} [m]
$\kappa_{\mathrm{s,M2}}$	Extensional stiffness 1 of a motor arm	1.0×10^{-3} [N/m]
$\kappa_{\mathrm{s,M3}}$	Extensional stiffness 2 of a motor arm	1.0×10^{-3} [N/m]
N_{h}	Number of heads represented by a single motor arm	8
N_{a}	Number of arms per motor	8
κ_{r}	Strength of repulsive force	1.69×10^{-3} [N/m]
C_{A}	Actin concentration	30 [μM]
R_{M}	Ratio of motor concentration to C_{A}	0.00125-0.64
R_{ACP}	Ratio of ACP concentration to C_{A}	0.00125-0.08
$<L_{\mathrm{f}}>$	Average length of F-actins	1.74 - 2.53 [μm]
Δt	Time step	1.15×10^{-5} [s]
μ	Viscosity of medium	8.6×10^{-1} [kg/m·s]
$k^{0}_{\mathrm{u,ACP}}$	Zero-force unbinding rate constant of ACP	0.115 [s^{-1}] ($=k^{0*}_{\mathrm{u,ACP}}$) [7]
$\lambda_{\mathrm{u,ACP}}$	Force sensitivity of ACP unbinding	1.04×10^{-10} [m] [7]
$k^{0}_{\mathrm{s,A}}$	Zero-angle severing rate constant	0 - 10^{-20} [s^{-1}]
$\lambda_{\mathrm{s,A}}$	Sensitivity of a severing rate to a bending angle	2.79×10^{-2} [rad]
$k_{\mathrm{B}}T$	Thermal energy	4.142×10^{-21} [J]

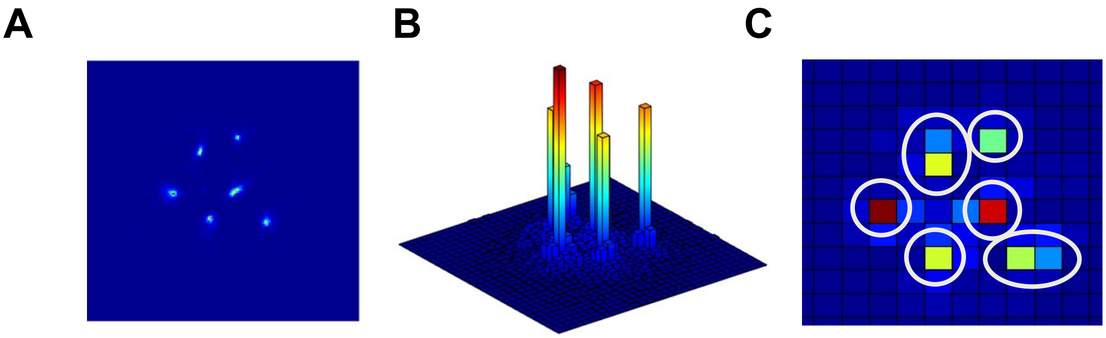

Fig. S1. The number of foci after contraction is automatically detected. (A) An example of the actin density map after full contraction from a simulation. (B) Three-dimensional histogram showing the actin density. (C) Non-blue points which are not adjacent to other non-blue points are considered separate foci. In this example, 6 foci are detected.

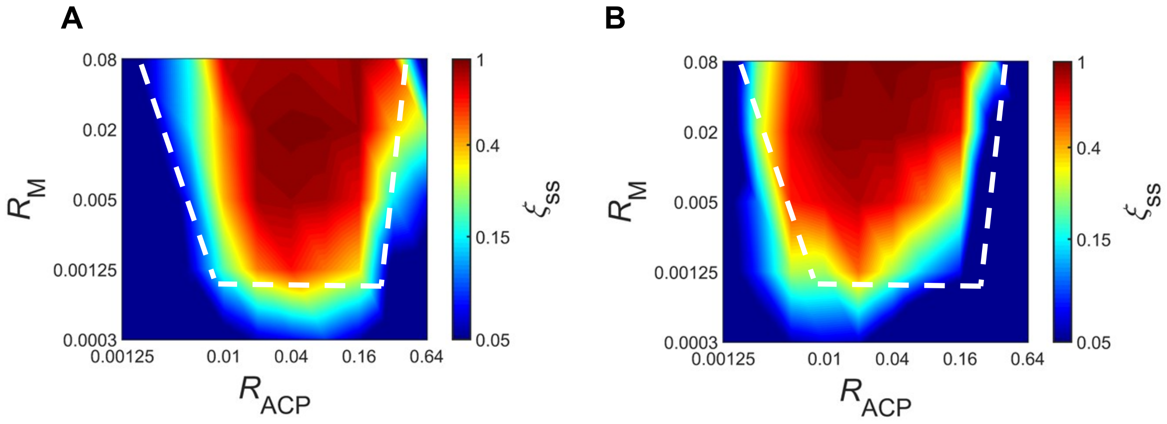

Fig. S2. Bending stiffness ($\kappa_{b,A}$) and length ($<L_f>$) of actin filaments modulate network contraction. (A) When $<L_f>$ is reduced from 2.53 μm to 1.74 μm, critical levels of R_{ACP} above which large contraction occurs are higher (c.f. Fig. 2C) because more ACPs are needed for the minimal network connectivity if the network has lower connectivity due to shorter actin filaments. (B) When $\kappa_{b,A}$ is increased 16-fold, the transition of contraction on the left still occurs at R_{ACP} ~ 0.0025-0.005. By contrast, the transition on the right takes place at lower R_{ACP} (c.f. Fig. 2C) because buckling of actin filaments requires a larger amount of forces (i.e. higher R_M) at each R_{ACP}. In (A-B), for comparison, red dashed lines indicate a regime where large network contraction emerges in Fig. 2C.

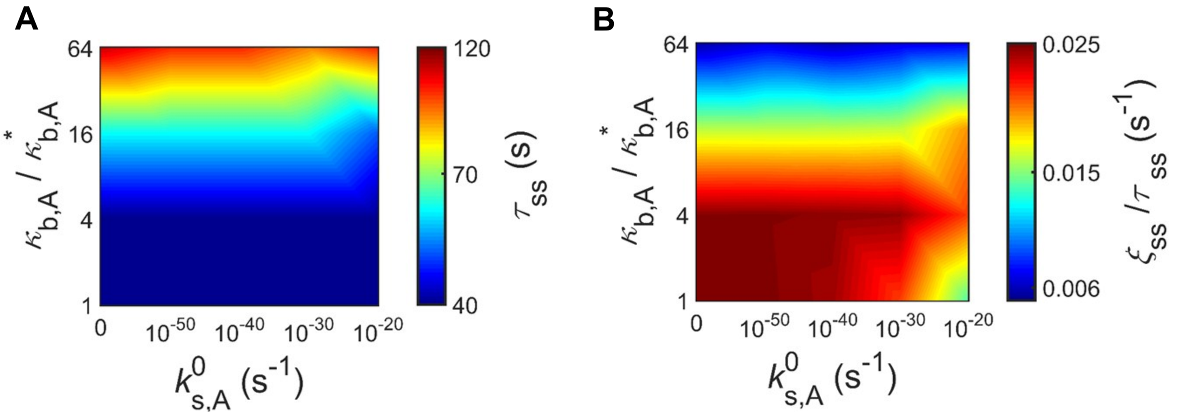

Fig. S3. (A) Time required for reaching the steady state of contraction (τ_{ss}) and (B) average contraction rate which corresponds to ξ_{ss} / τ_{ss}, at various $k^0_{s,A}$ and $\kappa_{b,A}$.

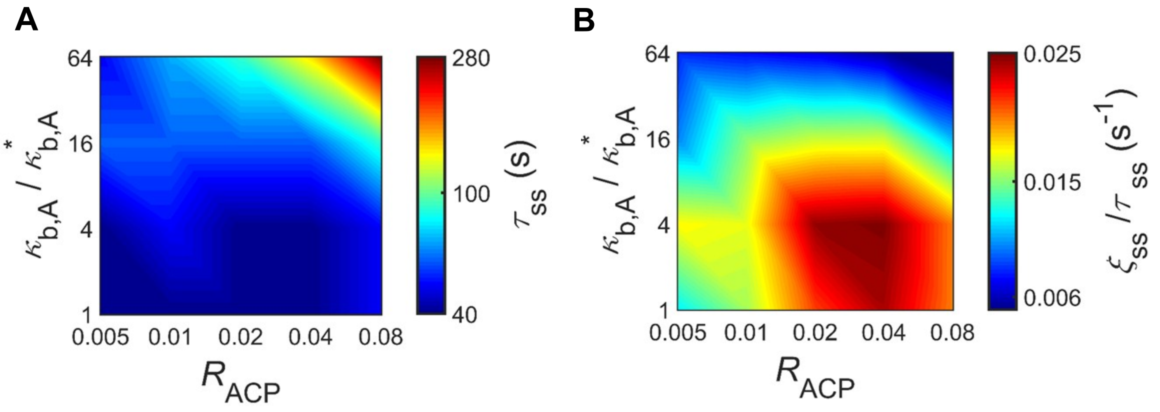

Fig. S4. (A) τ_{ss} and (B) average contraction rate over a wide range of R_{ACP} and $\kappa_{b,A}$.

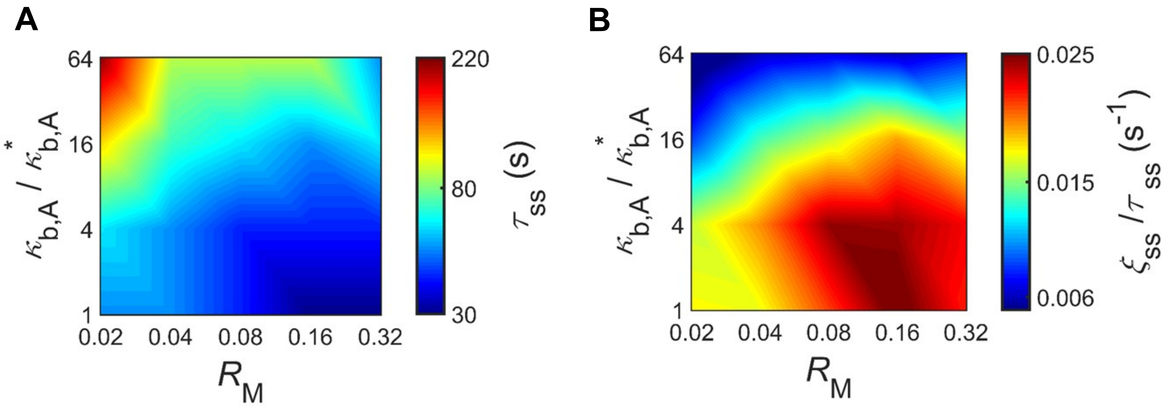

Fig. S5. (A) τ_{ss} and (B) average contraction rate at various R_M and $\kappa_{b,A}$.

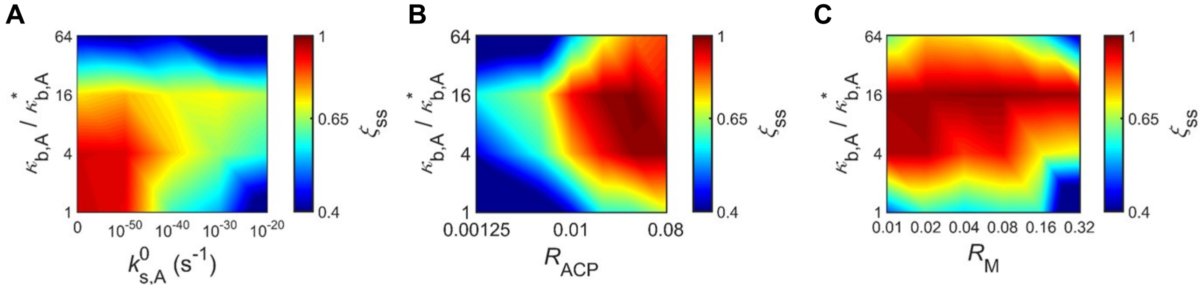

Fig. S6. The three-dimensional phase diagram in Fig. 6B is created by further exploration of parametric spaces. ξ_{ss} is measured under various conditions. (A) ξ_{ss} ($k^0_{s,A}$, $\kappa_{b,A}$) with R_{ACP} = 0.005 and R_M = 0.08. (lower R_{ACP} than that used in cases shown in Fig. 3D) (B) ξ_{ss} (R_{ACP}, $\kappa_{b,A}$) with $k^0_{s,A}$ = 10^{-20} s^{-1} and R_M = 0.08. (higher $k^0_{s,A}$ than that used in cases shown in Fig. 4D) (C) ξ_{ss} (R_M, $\kappa_{b,A}$) with $k^0_{s,A}$ = 10^{-20} s^{-1} and R_{ACP} = 0.02. (higher $k^0_{s,A}$ than that used in cases shown in Fig. 5D)

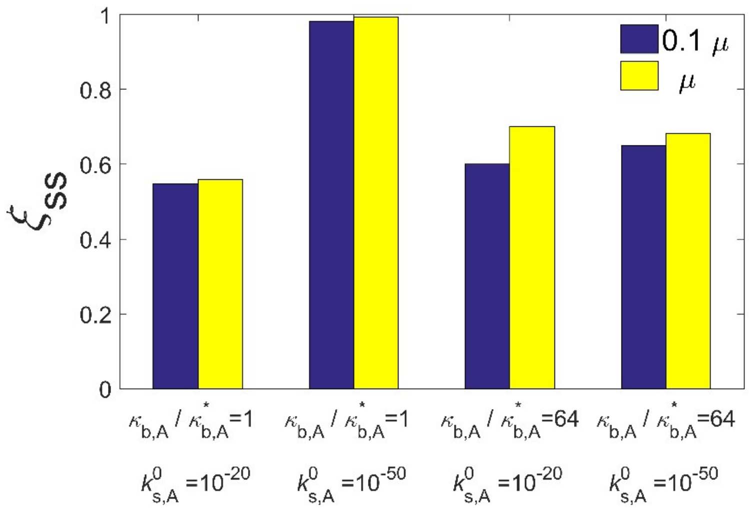

Fig. S7. Effects of the medium viscosity (μ) on ξ_{ss}. No significant differences in ξ_{ss} are observed between cases with $\mu = 8.6\times10^{-1}$ [kg/m·s] used in this study and those with $\mu = 8.6\times10^{-2}$ [kg/m·s] used in our previous study.

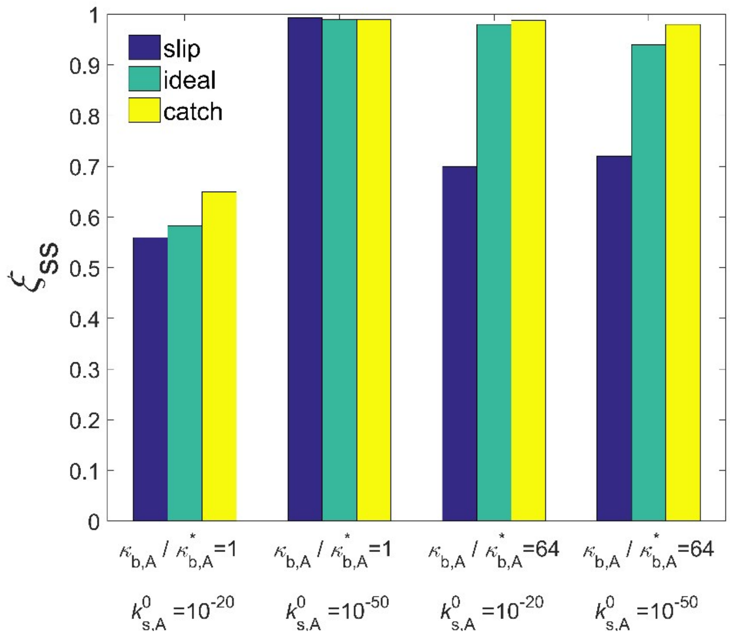

Fig. S8. Effects of force sensitivity of ACP unbinding on ξ_{ss}. ξ_{ss} is almost independent of the force sensitivity if $\kappa_{b,A}$ is small. However, if $\kappa_{b,A}$ is large, contraction is greater with catch-bond ACPs or ideal-bond ACPs.

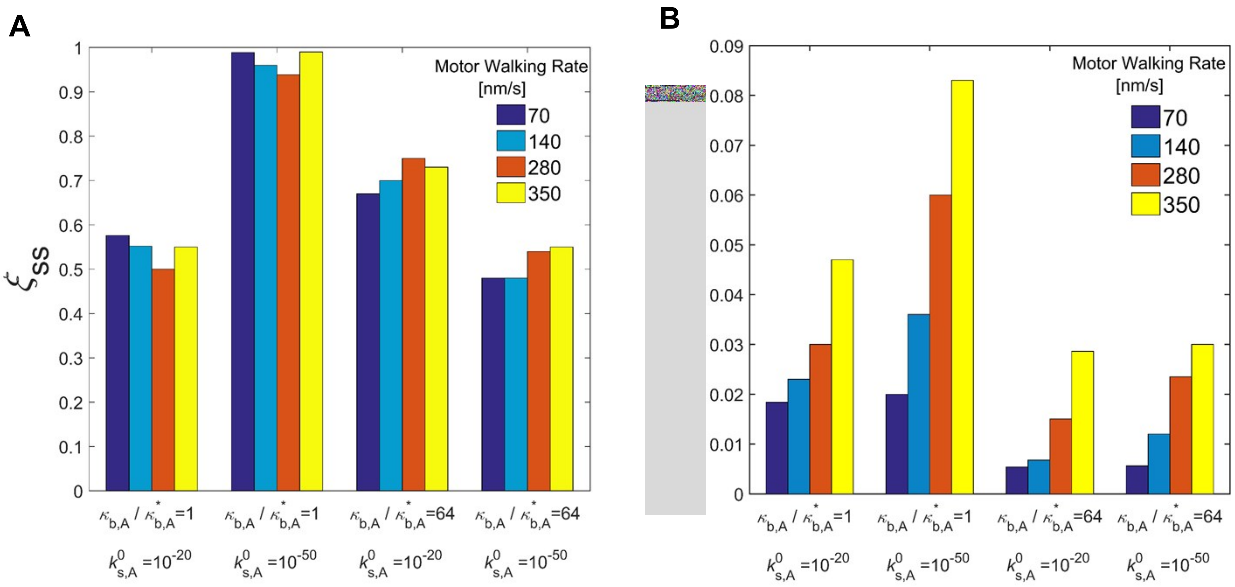

Fig. S9. Influences of motor walking rate ($k_{w,M}$) on ξ_{ss} and average contraction rate. (A) ξ_{ss} is almost independent of $k_{w,M}$. (B) The average contraction rate is proportional to $k_{w,M}$.

References

1 Underhill, P.T. and P.S. Doyle, On the coarse-graining of polymers into bead-spring chains. J Non-Newton Fluid, 2004. 122(1): 3-31.

2 Clift, R., J.R. Grace, and M.E. Weber, Bubbles, drops, and particles. 2005: Courier Corporation.

3 Jung, W., M.P. Michael, and T. Kim, F-actin fragmentation induces distinct mechanisms of stress relaxation in the actin cytoskeleton. ACS Macro Lett, 2016. 5: 641-5.

4 Isambert, H., et al., Flexibility of actin filaments derived from thermal fluctuations. Effect of bound nucleotide, phalloidin, and muscle regulatory proteins. J Biol Chem, 1995. 270(19): 11437-44.

5 Kim, T., et al., Computational analysis of viscoelastic properties of crosslinked actin networks. PLoS Comput Biol, 2009. 5(7): e1000439.

6 Bell, G.I., Models for the specific adhesion of cells to cells. Science, 1978. 200(4342): 618-27.

7 Ferrer, J.M., et al., Measuring molecular rupture forces between single actin filaments and actin-binding proteins. Proc Natl Acad Sci U S A, 2008. 105(27): 9221-

8 Erdmann, T. and U.S. Schwarz, Stochastic force generation by small ensembles of myosin II motors. Phys Rev Lett, 2012. 108(18): 188101.

9 Erdmann, T., P.J. Albert, and U.S. Schwarz, Stochastic dynamics of small ensembles of non-processive molecular motors: The parallel cluster model. J Chem Phys, 2013. 139(17): 175104.

10 Kim, T., Determinants of contractile forces generated in disorganized actomyosin bundles. Biomech Model Mechanobiol, 2015. 14(2): 345-55.

11 Plaza, G.R. and T.Q.P. Uyeda, Contraction speed of the actomyosin cytoskeleton in the absence of the cell membrane. Soft Matter, 2013. 9: 4390-400.

12 Kishino, A. and T. Yanagida, Force measurements by micromanipulation of a single actin filament by glass needles. Nature, 1988. 334(6177): 74-6.

13 Meyer, R.K. and U. Aebi, Bundling of actin filaments by alpha-actinin depends on its molecular length. J Cell Biol, 1990. 110(6): 2013-24.